Article

Integration of Stationary Batteries for Fast Charge EV Charging Stations

Davide De Simone * and Luigi Piegari

Dipartimento di Elettronica, Informazione e Bioingegneria, Politecnico di Milano, 20133 Milano, Italy; luigi.piegari@polimi.it

* Correspondence: davide.desimone@polimi.it

check for updates

Abstract: One of the biggest issues preventing the spread of electric vehicles is the difficulty in supporting distributed fast charging stations by actual distribution grids. Indeed, a significant amount of power is required for fast charging, especially if multiple vehicles must be supplied simultaneously. A possible solution to mitigate this problem is the installation of auxiliary batteries in the charging station to support the grid during high peak power demands. Nevertheless, the integration of high-voltage batteries with significant power is not a trivial task. This paper proposes the configuration and control of a converter to integrate batteries in a fast charging station. The proposed configuration makes it possible to decouple the grid power from the vehicle power using several auxiliary battery modules. At the same time, the converter makes it possible to draw different amounts of power from the battery modules, allowing the use of second life batteries performing in different ways. This paper discusses the design, control, and operation of the converter. Moreover, the effectiveness of the proposed control is shown by means of numerical results.

Keywords: battery electric vehicle; BEV; charging station; stationary storage; plug-in; EV; fast charge; power quality; second life batteries

1. Introduction

Electric vehicles (EVs) are spreading in the private transportation sector. Although these vehicles contribute less to city pollution, their spread is being hindered by limitations such as their high price, short range, and long recharge time compared to the equivalent category of internal combustion vehicles [1]. Battery technologies are being rapidly developed, with steady increases in their energy and power densities and decreases in their prices [2].

Higher power density batteries can accept higher recharging power levels, allowing a fast charge. Together with the spread of electric vehicles, the recharging infrastructure is undergoing significant development in terms of charging points and installed power. A generic EV power profile during the recharge phase is characterized by a high peak power demand that usually lasts 26–32 min [3]. Standard fast dc charging is performed at 50 kW dc, but multiple charging systems make it possible to charge at higher power. By 2021, fast charging up to 350 kW might be possible [4]. The most common charging standards and relative power ratings are summarized in Table 1 [4].

In urban areas, it is likely that many consumers will recharge their vehicles between 7:00 and 9:00, at noon, and between 18:00 and 20:00 [3,5]. Grid operators might not be able to overcome future peak power requirements without greatly oversizing the installed power. A possible approach to mitigate this problem might be to add a battery electric storage system (BESS) to a fast charging station (FSS), which will act as a buffer to reduce the peak power demand on the network without increasing the EV charging time.

Table 1. Charging standards.

System	kW	Availability
Combined Charging System (CCS)	50–350	United States European Union Australia, Korea
China GB/T	237.5	China, India
Tesla Supercharger	135	Global
CHAdeMO	50–100	Global

Two possible approaches could be followed to interface a BESS with a charging station [6]: ac coupling and dc coupling. In ac coupling, the storage system and charging converters are interconnected through an ac bus. In dc structures, the interconnection is through a common dc link. Figure 1 shows schematics of the two coupling methods.
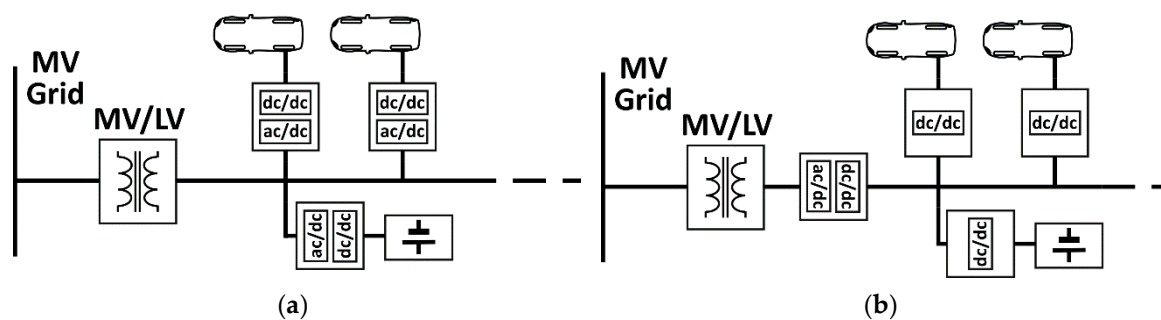
Figure 1. Charging station coupling methods: (**a**) ac coupling and (**b**) dc coupling.

At present, ac coupling is the most widespread because of the maturity of the ac technology in terms of the converter design, protection devices, and standards. Although ac coupling is more common, dc coupling provides a higher efficiency and lower cost because this configuration requires fewer conversion stages.

Modular multilevel converters (MMCs) are widely used in dc/ac medium/high-voltage applications. Their multilevel output waveform reduces the total harmonic content of the generated ac voltage and, thus, the harmonics the of ac currents are quite limited also using a very small filter. Depending on the number of levels and the grid impedance, a filter-less solution can be acceptable [7–10].

Double star chopper cells converters (DSCCs) replace the floating capacitors of traditional MMCs with a battery. Recently, the use of this converter in an electric vehicle powertrain has been proposed [11].

Embedding DSCCs in EVs offers some major advantages. The storage system is embedded inside the converter structure, which makes it possible to perform the battery management system (BMS) operations without dedicated hardware [11]. Moreover, it is possible to balance the batteries within each arm to exploit the load currents rather than moving energy from one cell to another, potentially making the process more efficient. The control strategies available in the literature make it possible to recharge the storage system [12] from any power source, i.e., ac three phase, ac single phase, and dc. Finally, the modular structure ensures a highly redundant system [13]. The DSCC structure also seems to be very promising for integrating a storage system in an EV charging station to support the grid during a peak power demand. Indeed, batteries can be integrated, at the module level, directly in the converter modules to ensure the correct power sharing between the modules. In this way, the power converter also operates as a BMS controlling the power exchanged individually by each battery module. Second life batteries can be used because each battery module is controlled separately from the others, and the modularity of the solution makes it possible to substitute only one battery module without the need to substitute all the others. With the proper choice of voltage levels, the dc bus of the DSCC can be used inside the EV station for fast dc charging.

This paper proposes the use of a DSCC converter to integrate an auxiliary storage system with an EV charging station. Moreover, a new control strategy to separately control the power exchanged by this converter at its dc and ac ports is proposed. This control strategy was simulated in a dc coupled charging station, and the results obtained show that is possible to meet the charging power demand by drawing constant power from the three-phase grid. In this way, the power installation required by the EV charging station is limited and lower than the power required by modern fast dc charging systems. This mitigates a big problem with modern fast charging systems, facilitating the diffusion of electric vehicles.

2. Materials and Methods

2.1. Converter Control

The investigated DSCC converter is composed of three phases, each one realized with two arms embedding six modules (Figure 2). The common points of the three phases are used to obtain a virtual dc bus. For each arm, the reference voltage is obtained as follows:

$$\begin{cases} v^*_{lower,k} = \frac{v^*_{dc}}{2} + v^*_{phase,k} + v^*_{circ,k} \\ v^*_{upper,k} = \frac{v^*_{dc}}{2} - v^*_{phase,k} + v^*_{circ,k} \end{cases} \tag{1}$$

where $v^*_{lower,k}$ and $v^*_{upper,k}$ are, respectively, the phase k lower and upper reference arm voltages. v^*_{dc} is the voltage reference for the dc bus of the converter, $v^*_{phase,k}$ is the phase voltage reference, and $v^*_{circ,k}$ is the output of the circulating current controller for phase k used to balance the battery cells of the upper and lower arms [13]. It is worth noting that the three virtual dc buses can have different reference voltages:

$$v^*_{dc,k} = v^*_{dc} + 2 \cdot v^*_{circ,k} \tag{2}$$

This is done to make it possible to balance the state of charge (SOC) of the battery cells of the three legs of the converter.

The modulation strategy must be able to control the dc bus voltage reference. In literature different modulation techniques for this converter topology are available. The modulation techniques can be divided in two categories: nearest level control technique (NLC) and pulse width modulation (PWM) based ones [14]. NLC approximates the output voltage by turning on and off modules in order to minimize the discretization error related to the voltages of the modules, while PWM techniques add a switching signal to the output of NLC. As a consequence, NLC has a discretization error on the dc bus voltage equal to one module voltage. Therefore, if the number of levels is not very high, it can be used neither for a precise control of the dc bus voltage nor for proper balancing among the phases. This is the reason why, in this paper a PWM based technique is used. Given the references for each arm voltage, the control signals of the converter modules are obtained using phase disposition pulse width modulation (PD-PWM) [15]. It is worth noting that the results of this paper can be obtained with any PWM based technique. The choice of the PD-PWM is only based on its simplicity of implementation. This modulation consists of comparing the references with multiple carriers, where the amplitude is the voltage module, translated from the voltages of the other connected modules to avoid overlapping among them, as shown qualitatively in Figure 3.

As the voltages of the battery modules are never perfectly matched, circulating currents might flow among the phases. Given the arm currents, referring to the symbols of Figure 2, the circulating currents ($i_{circ,k}$) and phase currents ($i_{phase,k}$) are defined as follows:

$$\begin{cases} i_{circ,k} = \frac{1}{2}\left(i_{upper,k} + i_{lower,k}\right) \\ i_{phase,k} = i_{upper,k} - i_{lower,k} \end{cases} \tag{3}$$

where $i_{upper,k}$ and $i_{lower,k}$ are the phase k arm currents. It is worth noting that the dc component of the circulating current is used to balance the batteries among the phases, while energy is exchanged between the upper and lower arms using the second harmonic component of the same circulating current. A dedicated circulating current controller is implemented to allow battery balancing among the arms and phases [13]. The leg and arm balance is achieved following [16]. The logic scheme of the circulating current controller is shown in Figure 4, where v_{ph} is the space vector of the phase voltages generated by the converter; i^*_{circ} is the reference space vector of the circulating currents; and $v^*_{circ,a}$, $v^*_{circ,b}$, and $v^*_{circ,c}$ are the dc bus references for each phase. In practice, the balancing is obtained with three different actions:

1. Balancing among battery modules belonging to same arm is achieved by sorting the cells on the basis of their SOC and using the most charged (discharged) when the current is discharging (charging) them;
2. Balancing among battery modules belonging to different legs is achieved by changing the dc reference voltage of each leg allowing the circulation of a dc current among the legs (this current does not interest the load);
3. Balancing among upper and lower arms is achieved using an oscillating zero-sequence current (equal on each phase) that takes more energy from the lower (upper) arm if this is the more charged.
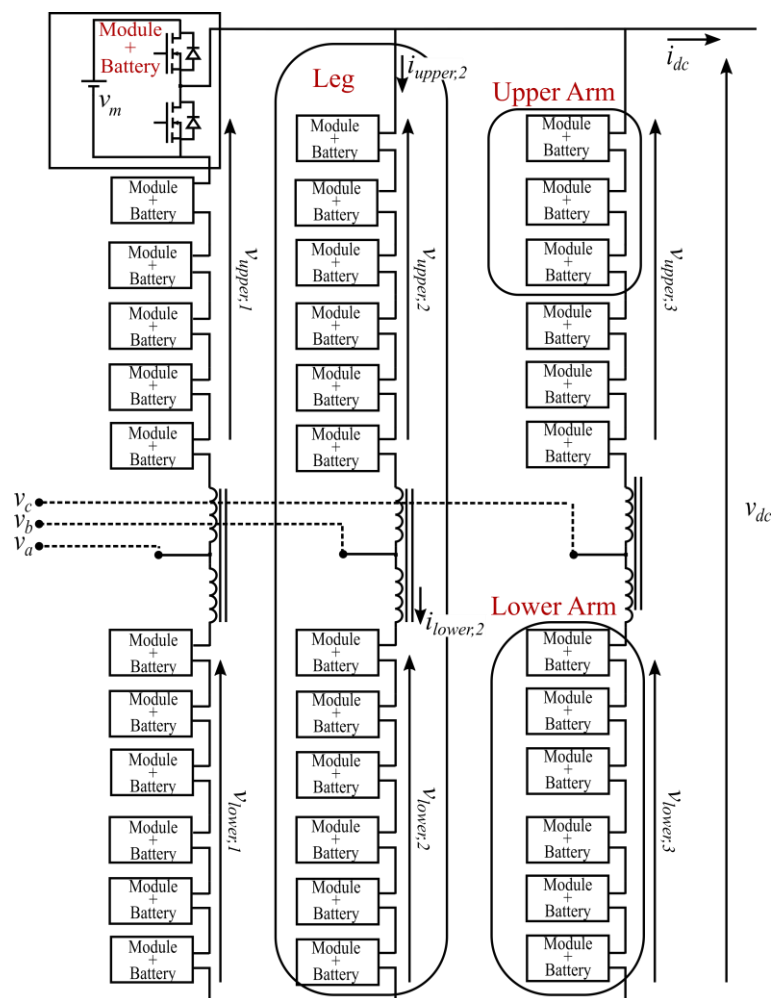

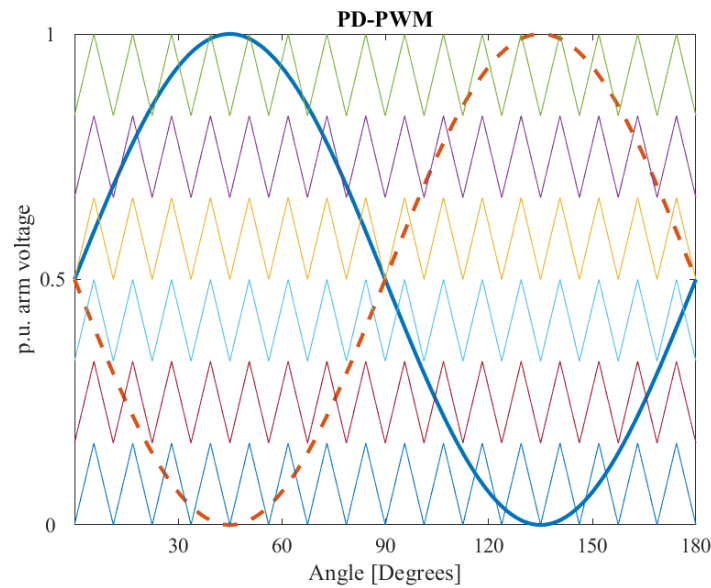**Figure 2.** Six modules per arm of the double star chopper cells converter (DSCC).

Figure 3. Phase disposition PWM (PD-PWM) qualitative modulation. Solid line: upper arm reference, dashed line: lower arm reference.
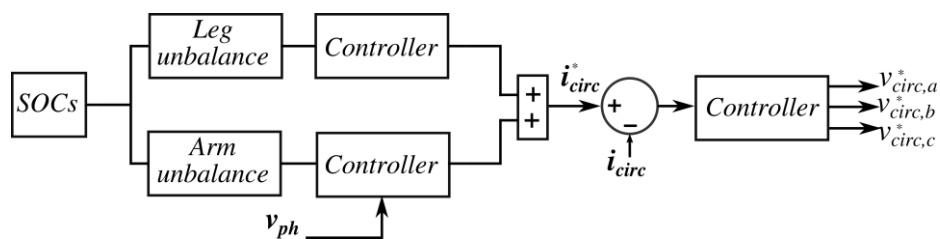

Figure 4. Leg and arm balance controllers. SOCs are all the modules' state of charge values. "Leg unbalance" computes the mean SOC of each phase and compares the results. "Arm unbalance" computes the imbalance between the upper and lower arms for each phase.

This balancing technique, anyway, is widely addressed in [16] and, therefore, it will not analyzed in more details in this paper.

In order to control the dc power output of the converter, a dedicated controller acts on the average dc bus voltage of the converter: reference dc current i^*_{dc} is computed given reference dc power P^*_{dc} and dc bus voltage v_{dc}. The difference between the reference and actual dc current, i_{dc}, is used for the input of the dc current regulator acting on the converter virtual dc bus voltage reference v^*_{dc}, as reported in Figure 5.
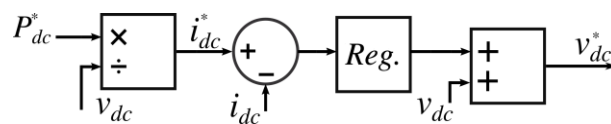

Figure 5. dc power regulator.

The ac power is controlled on a reference frame oriented on the grid voltage by means of a phase locked loop (PLL). On this reference frame, the controls of the active and reactive power are decoupled. Indeed, the direct axis oriented on the voltage space vector is indicated with "*d*" and the axis with a 90° lead is shown by "*q*", where the quadrature component of the voltage is equal to zero, resulting in the following [17,18]:

$$P_{ac} = \tfrac{3}{2}v_d i_d$$
$$Q_{ac} = \tfrac{3}{2}v_d i_q$$

(4)

Therefore, the control of the active power is obtained by dividing the active power reference P^*_{ac} by the direct component of the grid voltage vector, obtaining the direct current reference i^*_d. Using a multilevel converter, the filter impedance to connect to the ac grid is very low, and it is possible to control the direct and quadrature components of the current by directly controlling, respectively, the direct and quadrature components of the voltage produced by the converter.

The position of the voltage grid, $\angle\mathbf{v}_{ph}$, is then used to obtain the reference for the space vector of the voltage to be used for the converter. The simplified control scheme is reported in Figure 6.
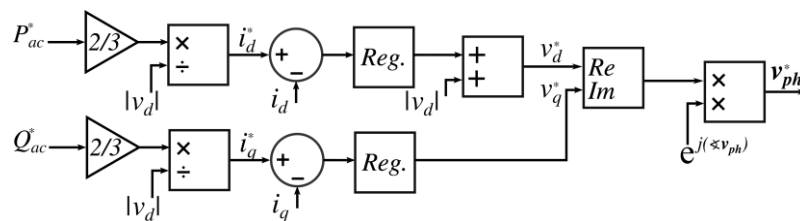

Figure 6. Active and reactive power regulator.

In [3] the charging station exchanges reactive power with the grid to provide grid services and increasing the profitability of the installation. If no requirements is given for the reactive power, its reference is usually set to zero to exchange power at unitary power factor minimizing the current and, consequently, the losses. A zero reference for the reactive power is assumed for this paper.

2.2. Converter Sizing

Acting separately on the ac and dc power references, it is possible to simultaneously control the dc and ac active power levels. The difference between the two is automatically stored or supplied by the storage system. To simultaneously control the two power levels, the voltage levels of the converter must be chosen so that the two controllers do not interact with each other. In particular, the lowest voltage on the dc bus to regulate the power flows must be higher than the EV battery voltages and, at the same time, it has to be higher than twice the highest voltage that is required on the ac side.

Allowing a voltage variation on the ac side of ±10% and considering an additional ±10% margin to allow the control of the reactive power, the ac output voltage of the converter has to be able to reach a value that is 20% higher than the rated ac voltage. As a consequence, to allow the full controllability on the ac side, the minimum dc voltage $v_{dc,min}$ is as follows:

$$v_{dc,min} = 2 \cdot 1.2 \cdot v_{ph,rated} \tag{5}$$

where $v_{ph,rated}$ is the peak of the rated grid voltage. If a ±10% margin is considered for the regulation of the dc power and the balancing among the phases, the minimum module voltage $v_{module,min}$ can be calculated as follows:

$$v_{module,min} = \frac{1.1 v_{dc,min}}{n_{modules}} \tag{6}$$

where $n_{modules}$ is the number of modules per arm. In [3], a charging station with a storage system was dimensioned so that the batteries' SOC did not go below 20% under normal working conditions. The minimum number of cells in the stack is thus obtained by applying the following:

$$n_{stack} = \left\lceil \frac{v_{module,min}}{v_{cell,min}} \right\rceil \tag{7}$$

where $v_{cell,min}$ is the minimum voltage achieved by one battery cell at the lowest SOC limit.

In this article, three vehicles of different categories are considered: the BMW i3 (EV_1), belonging to the city car category; the Nissan Leaf e+ (EV_2), representing a medium size vehicle; and finally, the

Porsche Taycan (EV_3), which is a sports car. Their storage systems and charging power specifications are summarized in Table 2 [4,19–21].

Table 2. Considered vehicles' specifications.

	Vehicle	Usable Battery Capacity (kWh)	Charging Power (kW)
EV_1	BMW i3	37.9	46
EV_2	Nissan Leaf e+	56	100
EV_3	Porsche Taycan	83.7	350

The charging station is supposed to have one fast charging dc port for the vehicles. It draws power from a 100 kW three-phase low-voltage grid. Each vehicle is supposed to arrive at the charging spot with a 10% SOC. The end of charge is considered at a SOC of 90%. As shown in [3], the average time, t_{swap} necessary to connect the charging station to the next customer is 10 min. To grant the maximum charging power to the vehicles, the stationary storage system is dimensioned to be able to recharge the medium size and large EVs in a row. The energy that must be stored is given by the energy balance between the network and the vehicles:

$$E_{storage} = \frac{1}{0.6} \cdot \frac{1}{\eta} \left\{ 0.8 \cdot (E_{EV,2} + E_{EV,3}) - P_{network} \cdot \left[0.8 \cdot \left(\frac{E_{EV,2}}{P_{EV,2}} + \frac{E_{EV,3}}{P_{EV,3}} \right) + \frac{t_{swap}}{60} \right] \right\} \tag{8}$$

where 0.6 represents the exploited energy of the stationary storage (20%–80%); η is the global efficiency of the storage and converter, which is supposed to be 90%; $E_{EV,k}$ and $P_{EV,k}$ are, respectively, the battery rated energy in Wh and the charging power in W of the k vehicle, while t_{swap} is expressed in minutes.

The power exchange with the grid is managed in order to keep the stationary storage system SOC below 80% and to not overcome the power limit of 100 kW. If the vehicle is being charged at less than 100 kW and the stationary storage reaches 80%, the network power is reduced to match the vehicle power demand. The dc power controller instead is programmed to prevent the storage system from reaching a SOC lower than 20%. If a vehicle whose charging power is higher than the grid power is connected, the dc power will be the maximum allowed until the storage system reaches a minimum SOC (SOC_{min}) of 20%; then the dc power is limited to the power from the grid. To generate the dc power reference, the stationary battery SOC_{min} is compared with the minimum allowed SOC of 20%. The result is given as an input to a regulator whose output is saturated between the minimum and maximum dc power levels of the installed DSCC. The result is that the maximum dc power $P_{dc,max}$ is compatible with the current SOC_{min}. The dc power required by the vehicle is then saturated between 0 and $P_{dc,max}$. The schematic of the minimum SOC regulator is reported in Figure 7.
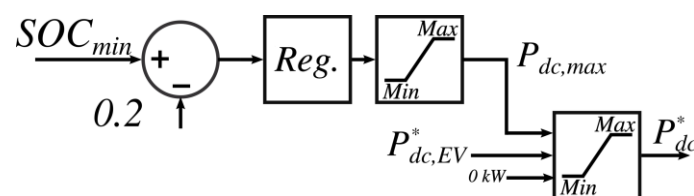

Figure 7. Min SOC regulator.

The ac power reference is generated by comparing the average SOC with the maximum allowed SOC of 80%. The result is given to a regulator whose output is saturated between 0 and the maximum ac power, i.e., 100 kW (Figure 8).
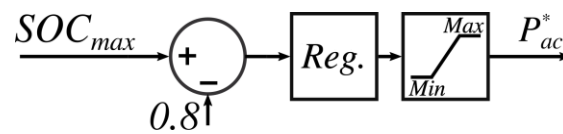
Figure 8. Max SOC regulator.

2.3. Test Setup

The proposed control strategy was tested by simulating the continuous connection of the vehicles one after the other with pauses of 10 min between subsequent connections (as shown in Figure 9b).
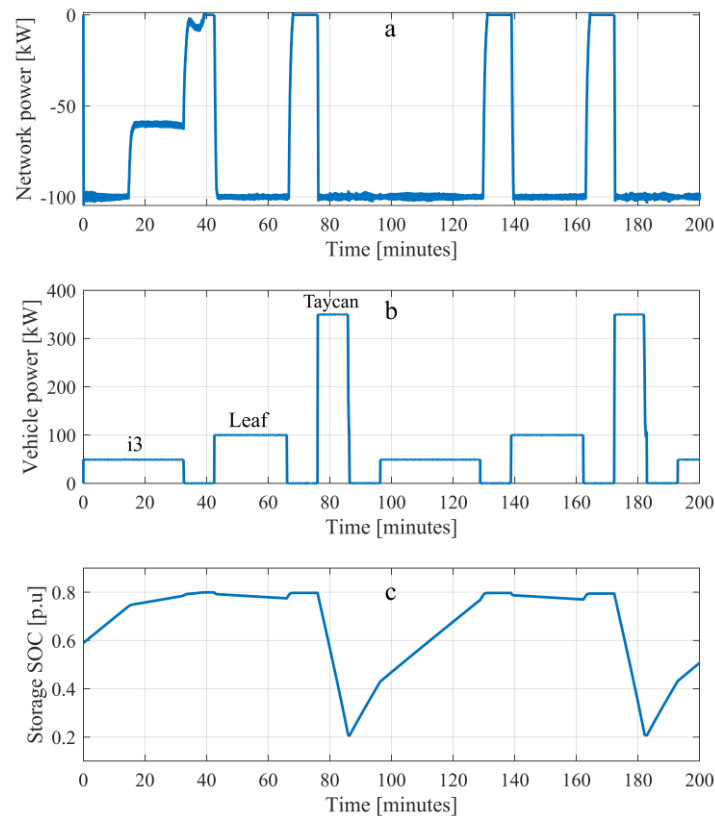

Figure 9. Simulation results: (**a**) grid power, (**b**) vehicle power, and (**c**) average SOC of stationary battery.

The initial average SOC of the charging station battery was considered to be 60%. To test the BMS capabilities, all of the modules were initialized with random SOCs between 40% and 80%.

3. Results

The control strategy was validated using Simulink. Figure 9 shows that the ac and dc power levels could be controlled separately by exploiting the DSCC storage system as an energy buffer, recharging the vehicles at their full capabilities without overloading the grid.

Comparing Table 3 with Table 2, it is possible to state that the full charging power capabilities were achieved even though the stationary storage system had a lower capacity than the highest-range vehicle. Moreover, the stationary storage was sized to maximize its expected lifespan using only an SOC range of 20%–80%.

In Figure 10, it is possible to analyze the effectiveness of the module balancing algorithm. Even if the starting condition represents a very unbalanced situation, the BMS capabilities of the DSCC topology allows the cells to be balanced without dedicated hardware in the first 40 min. From the

analysis of the figure, it is clear that, in the first 5 min, the balancing inside each arm is completed by using the load current.

Table 3. Summary of the parameters used for the simulations.

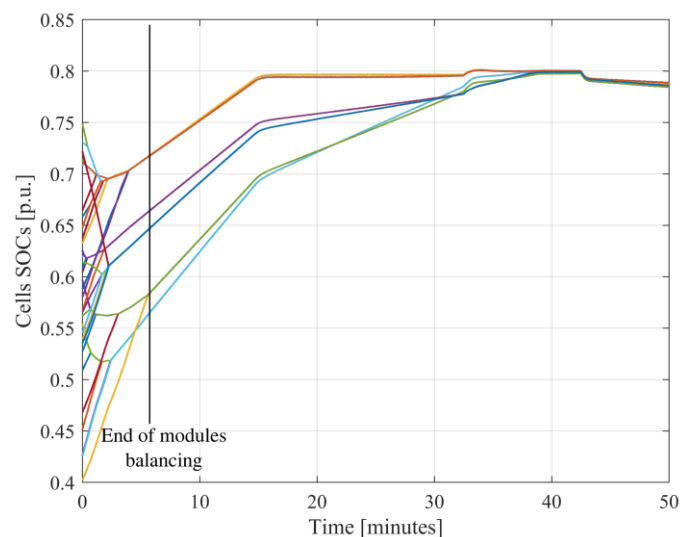| Converter Parameters		
Parameter	**Value**	**Meas. Unit**
$v_{ph,rated}$	311	V
$v_{cell,min}$	3	V
$v_{dc,min}$	828	V
$n_{modules}$	6	
n_{stack}	46	
$v_{module,min}$	138	V
$E_{storage}$	69	kWh

Figure 10. Modules' SOCs.

Then, in a longer time of up to 40 min, the balancing among the arms is achieved. As the arm balancing relies on the injection of circulating currents, the balancing power can be set to maximize the efficiency or reduce the balancing time. It is worth noting that SOCs of all the modules is always kept under the limit of 80% following the control rule presented in Section 3.

4. Discussion

At present, the main obstacles to the diffusion of EVs are their high costs, limited vehicle ranges, and long recharging times. In the future, several efforts will be devoted to increase the vehicle range while reducing the recharging time. For this reason, increasingly higher power levels will be required for charging stations. Nevertheless, the widespread requests for high-power nodes represent a critical scenario for actual electric transmission and distribution grids. For this reason, the option to add a local storage system in proximity to a fast charging station has been under analysis in the recent literature. In this paper, a new configuration to integrate battery modules in a fast charging station was proposed and studied. In particular, a DSCC power converter was used to achieve the following goals: (i) increasing the dc output voltage using lower voltage battery modules and (ii) balancing the battery modules by separately controlling the power drawn by each module, allowing the use of second life batteries. Moreover, a control strategy for the power converter was proposed in order to

decouple the control of the ac and dc power values exchanged by the converter. With the proposed control, it is possible to exchange two different power values on the two ports of the converter, and the power difference is automatically supplied or drawn by the stationary battery. In this way, it is possible to increase the power available for the fast charging station, requiring only the average power from the grid.

In this study, a power converter was modeled, and numerical results were obtained for a single point fast charging station. A sequence of three different kinds of vehicles, one city car, one medium-size car, and one sports car, were simulated, and the obtained numerical results showed the effectiveness of the proposed converter and strategy. Moreover, the balancing capabilities of the power converter were demonstrated.

References

1. Hoimoja, H.; Rufer, A.; Dziechciaruk, G.; Vezzini, A. An ultrafast EV charging station demonstrator. In Proceedings of the International Symposium on Power Electronics Power Electronics, Electrical Drives, Automation and Motion, Sorrento, Italy, 20–22 June 2012; pp. 1390–1395.
2. Overview of Battery Cell Technologies, Marcel MEEUS. Energy Materials Industrial Research Initiative (EMIRI). Available online: https://europa.eu/sinapse/webservices/dsp_export_attachement.cfm?CMTY_ID=0C46BEEC-C689-9F80-54C7DD45358D29FB&OBJECT_ID=230DABFD-90AB-8F7D-083EF5BD909DD025&DOC_ID=9C5B91FE-01BC-5F72-79D01E1939A9EE53&type=CMTY_CAL (accessed on 8 October 2019).
3. Richard, L.; Petit, M. Fast charging station with battery storage system for EV: Grid services and battery degradation. In Proceedings of the 2018 IEEE International Energy Conference (ENERGYCON), Limassol, Cyprus, 3–7 June 2018; pp. 1–6.
4. Voelcker, J. Porsche's fast-charge power play: The new, all-electric Taycan will come with a mighty thirst. This charging technology will slake it. *IEEE Spectr.* **2019**, *56*, 30–37. [CrossRef]
5. Jochem, P.; Landes, P.; Reuter-Oppermann, M.; Fichtner, W. Workload Patterns of Fast Charging Stations Along the German Autobahn. *World Electr. Veh. J.* **2016**, *8*, 936–942. [CrossRef]
6. Srdic, S.; Lukic, S. Toward Extreme Fast Charging: Challenges and Opportunities in Directly Connecting to Medium-Voltage Line. *IEEE Electrif. Mag.* **2019**, *7*, 22–31. [CrossRef]
7. Martinez-Rodrigo, F.; Ramirez, D.; Rey-Boue A., B.; de Pablo, S.; Herrero-de Lucas L., C. Modular Multilevel Converters: Control and Applications. *Energies* **2017**, *10*, 1709. [CrossRef]
8. Van Hertem, D.; Gomis-Bellmunt, O.; Liang, J. *HVDC Grids: For Offshore and Supergrid of the Future*; John Wiley & Sons: New York, NY, USA, 2016.
9. Li, J.; Bhattacharya, S.; Huang, A.Q. A New Nine-Level Active NPC (ANPC) Converter for Grid Connection of Large Wind Turbines for Distributed Generation. *IEEE Trans. Power Electron.* **2011**, *26*, 961–972. [CrossRef]
10. Ruderman, A.; Reznikov, B. Time domain evaluation of filterless grid-connected multilevel PWM converter voltage quality. In Proceedings of the 2010 IEEE International Symposium on Industrial Electronics, Bari, Italy, 4–7 July 2010; pp. 2940–2945.
11. D'Arco, S.; Piegari, L.; Tricoli, P. A modular converter with embedded battery cell balancing for electric vehicles. In Proceedings of the 2012 Electrical Systems for Aircraft, Railway and Ship Propulsion, Bologna, Italy, 16–18 October 2012; pp. 1–6.
12. D'Arco, S.; Quraan, M.; Tricoli, P.; Piegari, L. Battery charging for electric vehicles with modular multilevel traction drives. In Proceedings of the 7th IET International Conference on Power Electronics, Machines and Drives (PEMD 2014), Manchester, UK, 8–10 April 2014; p. 2.
13. Quraan, M.; Yeo, T.; Tricoli, P. Design and Control of Modular Multilevel Converters for Battery Electric Vehicles. *IEEE Trans. Power Electron.* **2015**, *31*, 507–517. [CrossRef]

14. De Simone, D.; Piegari, L.; D'Areo, S. Comparative Analysis of Modulation Techniques for Modular Multilevel Converters in Traction Drives. In Proceedings of the 2018 International Symposium on Power Electronics, Electrical Drives, Automation and Motion (SPEEDAM), Amalfi, Italy, 20–22 June 2018; pp. 593–600.

15. Ouerdani, I.; Bennani, A.; Ben, A.; Slama, B.; Montesinos Miracle, D. Phase Opposition Disposition PWM Strategy and Capacitor Voltage Control for Modular Multilevel Converters. In Proceedings of the International Conference on Recent Advances in Electrical Systems, Hammamet, Tunisia, 20–22 December 2016.

16. Brando, G.; Dannier, A.; Spina, I.; Tricoli, P. Integrated BMS-MMC Balancing Technique Highlighted by a Novel Space-Vector Based Approach for BEVs Application. *Energies* **2017**, *10*, 1628. [CrossRef]

17. Zahoor, W.; Zaidi, S.H. Synchronization and dq current control of grid-connected voltage source inverter. In Proceedings of the 17th IEEE International Multi Topic Conference 2014, Karachi, Pakistan, 8–10 December 2014; pp. 462–466.

18. Piegari, L.; Tricoli, P. A control algorithm of power converters in smart-grids for providing uninterruptible ancillary services. In Proceedings of the 14th International Conference on Harmonics and Quality of Power - ICHQP 2010, Bergamo, Italy, 26–29 September 2010; pp. 1–7.

19. Electric Vehicle Database. Available online: https://ev-database.org/car/1145/BMW-i3-120-Ah (accessed on 30 September 2019).

20. Electric Vehicle Database. Available online: https://ev-database.org/car/1144/Nissan-Leaf-eplus (accessed on 30 September 2019).

21. Electric Vehicle Database. Available online: https://ev-database.org/car/1116/Porsche-Taycan-Turbo-S (accessed on 30 September 2019).